RESEARCH PAPER

Channels 8:6, 509–518; November/December 2014; Published with license by Taylor & Francis Group, LLC

Caffeine-induced Ca^{2+} oscillations in type I horizontal cell of carp retina: A mathematical model

Ting Lv, Pu-Ming Zhang, Hai-Qing Gong, and Pei-Ji Liang

School of Biomedical Engineering; Shanghai Jiao Tong University; Shanghai, China

Keywords: Ca^{2+} oscillations, caffeine, computational model, retinal horizontal cell, ryanodine receptor, store-operated channel

Abbreviations: 2-APB, 2-Aminoethoxydiphenyl borate; $[Ca^{2+}]_{ER}$, Free Ca^{2+} concentration inside the lumen of the ER; $[Ca^{2+}]_i$, Intracellular free Ca^{2+} concentration; ANOVA, Analysis of variance; CICR, Ca^{2+}-induced Ca^{2+} release; ER, Endoplasmic reticulum; H1 HC, Type I horizontal cell; HC, Horizontal cell; L-VGCC, Ca^{2+}channel; NCX, Na^+/Ca^{2+} exchanger; PM, Plasma membrane; PMCA, Plasma membrane Ca^{2+}-ATPase; RyR, Ryanodine receptor; SERCA, Sarco/endoplasmic reticulum Ca^{2+}-ATPase; SNK, Student-Newman-Keuls; SOC, Store-operated channel; SOCE, Store-operated Ca^{2+} entry; STIM, Stromal interaction molecule; TRP, Transient receptor potential.

Oscillations in intracellular free Ca^{2+} concentration ($[Ca^{2+}]_i$) have been observed in a variety of cell types. In the present study, we constructed a mathematical model to simulate the caffeine-induced $[Ca^{2+}]_i$ oscillations based on experimental data obtained from isolated type I horizontal cell of carp retina. The results of model analysis confirm the notion that the caffeine-induced $[Ca^{2+}]_i$ oscillations involve a number of cytoplasmic and endoplasmic Ca^{2+} processes that interact with each other. Using this model, we evaluated the importance of store-operated channel (SOC) in caffeine-induced $[Ca^{2+}]_i$ oscillations. The model suggests that store-operated Ca^{2+} entry (SOCE) is elicited upon depletion of the endoplasmic reticulum (ER). When the SOC conductance is set to 0, caffeine-induced $[Ca^{2+}]_i$ oscillations are abolished, which agrees with the experimental observation that $[Ca^{2+}]_i$ oscillations were abolished when SOC was blocked pharmacologically, verifying that SOC is necessary for sustained $[Ca^{2+}]_i$ oscillations.

Introduction

$[Ca^{2+}]_i$ oscillations have been observed in a variety of cell types.[1] The present study is focused on caffeine-induced $[Ca^{2+}]_i$ oscillations in type I horizontal cell (H1 HC) of carp retina. Horizontal cells are interneurons in vertebrate retinas, which receive glutamate input from photoreceptors. In carp H1 HC, $[Ca^{2+}]_i$ increase is caused primarily by Ca^{2+} release from intracellular Ca^{2+} store (basically the endoplasmic reticulum, ER) via ryanodine receptor (RyR) activation[2,3] and Ca^{2+} influx from the extracellular environment, while Ca^{2+} removal depends on the activities of the sarco/endoplasmic reticulum Ca^{2+}-ATPase (SERCA),[2-4] Na^+/Ca^{2+} exchanger (NCX)[5] and plasma membrane Ca^{2+}-ATPase (PMCA).[5]

Ca^{2+} imaging study with carp H1 HC revealed that $[Ca^{2+}]_i$ oscillations could be induced when caffeine was applied at various concentrations.[6] The application of caffeine activates RyR, leading to ER Ca^{2+} release and ER depletion. Subsequent ER refilling, which should be required for the maintenance of $[Ca^{2+}]_i$ oscillations, is dependent on Ca^{2+} entry via store-operated channel (SOC). Hence RyR and SOC, together with the Ca^{2+} removal processes are the major components for caffeine-induced $[Ca^{2+}]_i$ oscillations. However, how these components interact with each other to give rise to $[Ca^{2+}]_i$ oscillations observed in H1 HC is unclear.

In the present study, a computational model based on biophysical properties of H1 HC was constructed to explore the underlying mechanism(s) of caffeine-induced $[Ca^{2+}]_i$ oscillations observed in H1 HC of carp retina. Using this model, caffeine-induced $[Ca^{2+}]_i$ oscillations were simulated. The concentration-dependent caffeine effect on the pattern of $[Ca^{2+}]_i$ oscillations was explored, relevant contributions of RyR, SOC, L-type voltage-gated Ca^{2+} channel (L-VGCC), NCX, PMCA and SERCA for caffeine-induced $[Ca^{2+}]_i$ oscillations were suggested, and the importance of SOC in caffeine-induced $[Ca^{2+}]_i$ oscillations was evaluated.

Results

Simulating caffeine-induced $[Ca^{2+}]_i$ oscillations in isolated H1 HC

Figure 1A–C shows the experimental observations of caffeine-induced $[Ca^{2+}]_i$ oscillations of 3 representative H1 HCs in

Correspondence to: Pei-Ji Liang; Email: pjliang@sjtu.edu.cn
Submitted: 07/26/2014; Revised: 09/05/2014; Accepted: 09/10/2014
http://dx.doi.org/10.4161/19336950.2014.965113

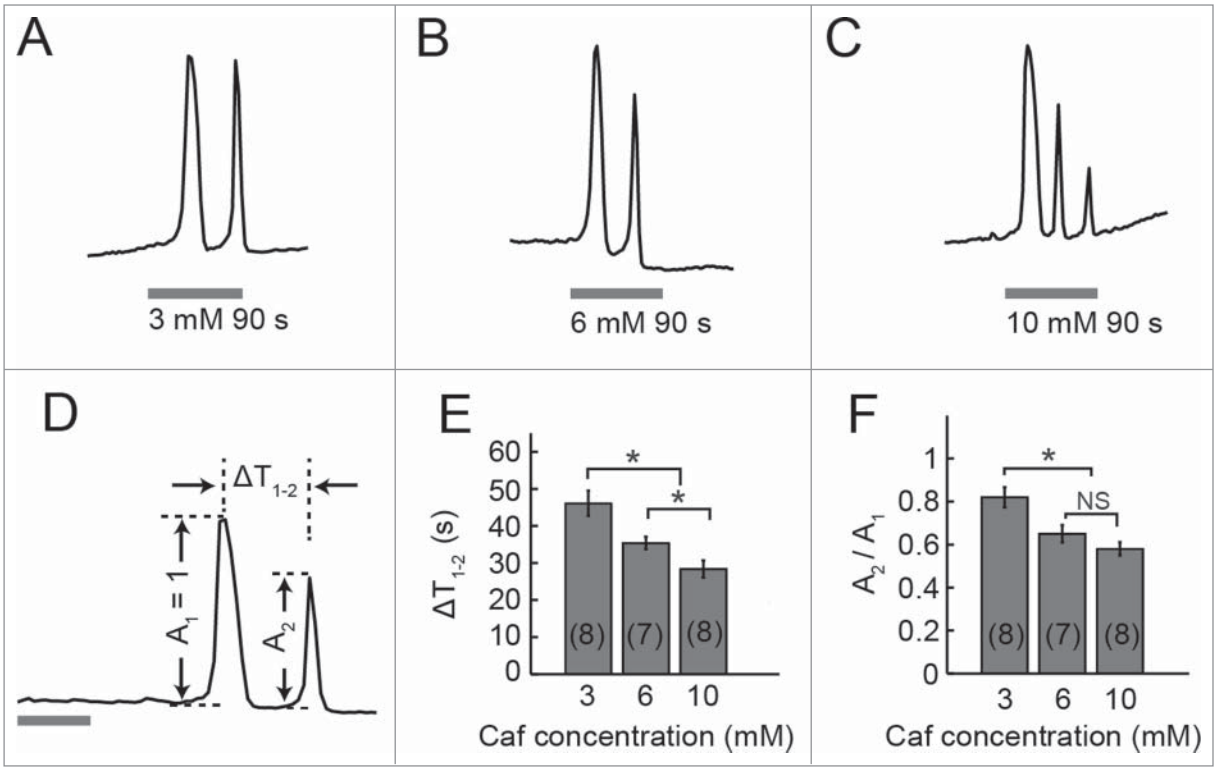

Figure 1. Concentration-dependent caffeine effects on the caffeine-induced $[Ca^{2+}]_i$ oscillations. (**A–C**) $[Ca^{2+}]_i$ oscillations induced by the application of 3, 6, and 10 mM caffeine (90 s), respectively. Horizontal bars bellow the traces indicate the periods of caffeine applications. (**D**) Definition of time interval between the first and the second Ca^{2+} transients ($\Delta T_{1\text{-}2}$) and the amplitude of the first and the second Ca^{2+} transients. (**E**) $\Delta T_{1\text{-}2}$ was decreased with caffeine concentration. (**F**) A_2/A_1 ratio was decreased with caffeine concentration. Data are presented as mean ± SEM (with sample size in parentheses). *denotes statistical significance of $P < 0.05$ by one-way ANOVA followed by post hoc SNK test, NS: not significant.[6]

response to 3, 6, 10 mM caffeine (with identical caffeine application time of 90 s), respectively.[6] Statistical results of the experimental data show that, when the concentration of caffeine was increased from 3 to 10 mM, the time interval between the first and the second Ca^{2+} transients ($\Delta T_{1\text{-}2}$; **Fig. 1D**) was decreased from 46.08 ± 3.41 s to 28.37 ± 2.30 s ($P < 0.05$, ANOVA, post hoc SNK test; **Fig. 1E**). The amplitude decrement during the Ca^{2+} oscillations was also concentration dependent. To quantify such amplitude decrement, the amplitude of the second transient was normalized against that of the first one (A_2/A_1; **Fig. 1D**). When caffeine concentration was increased from 3 to 10 mM, the normalized amplitude of the second transient (A_2/A_1) was decreased from 0.82 ± 0.05 to 0.58 ± 0.03 ($P < 0.05$, ANOVA, post hoc SNK test; **Fig. 1F**).[6]

Caffeine-induced $[Ca^{2+}]_i$ oscillations can be attributed to a number of factors (**Fig. 6**). Using the model cell, $[Ca^{2+}]_i$ oscillations induced by 3, 6, 10 mM caffeine were simulated (**Fig. 2A–C**) with parameter values listed in **Table 3 and 4**. The positive currents reflect Ca^{2+} efflux from cytoplasm to external environment or Ca^{2+} entering the ER.

Caffeine induces ER Ca^{2+} release by increasing the open probability of RyR (P_{RyR}), and P_{RyR} is increased when the concentration of caffeine is increased.[7,8] To simulate the caffeine effect on $[Ca^{2+}]_i$, the RyR activation constant ($K_{d,Ca}$ in **Eq. 10**), which reflects the RyR's sensitivity to Ca^{2+}, was adjusted. $[Ca^{2+}]_i$ responses induced by 3, 6, 10 mM caffeine were simulated with $K_{d,Ca}$ of 0.16, 0.14, 0.13 μM, respectively. The simulated $[Ca^{2+}]_i$ curves closely resemble the experimental observations (**Fig. 2A–C**).

Model output simulating $[Ca^{2+}]_i$ oscillations induced by 3 mM caffeine is shown in **Figure 2A**. Upon caffeine (3 mM) application, RyR current is increased immediately, leading to an increase in $[Ca^{2+}]_i$ and a decrease in free Ca^{2+} concentration inside the lumen of the ER ($[Ca^{2+}]_{ER}$). Currents carried by PMCA, NCX, and SERCA are increased accordingly, which bring $[Ca^{2+}]_i$ back to the basal level, forming the first $[Ca^{2+}]_i$ transient (the relative contributions of PMCA and NCX are illustrated in the insets of **Fig. 2A**). Meanwhile, SOC current is increased slowly upon ER depletion, which leads to a gradual ER refilling. RyR current is increased slowly with the increasing $[Ca^{2+}]_{ER}$, results in an increase in $[Ca^{2+}]_i$, which further potentiates the RyR current. Once sufficient amount of RyRs are activated, Ca^{2+} recycled by ER is again released, forming the subsequent $[Ca^{2+}]_i$ transient. During caffeine application, periodical changes in $[Ca^{2+}]_i$ is concomitant with the periodical activities of the RyR, PMCA, NCX, SERCA, SOC, and L-VGCC. After caffeine removal, each Ca^{2+} process returns to the resting state.

Figure 2B and C show model output induced by 6 and 10 mM caffeine, respectively. During 6 mM and 10 mM

caffeine applications, the overall patterns of dynamic changes in $[Ca^{2+}]_i$, $[Ca^{2+}]_{ER}$ and Ca^{2+} currents are similar to that during 3 mM caffeine application.

By comparing simulated $[Ca^{2+}]_i$ curves with 3, 6, and 10 mM caffeine, it is shown that $[Ca^{2+}]_i$ signal is caffeine concentration dependent. We also calculated the values of $\Delta T_{1\text{-}2}$ and A_2/A_1 with each caffeine concentration (**Table 1**). Results show that when the concentration of caffeine is increased from 3 mM to 10 mM, the $\Delta T_{1\text{-}2}$ interval is decreased from 56.72 s to 38.46 s, and the A_2/A_1 ratio is decreased from 0.81 to 0.54, both in accordance with the experimental observations.

By examining the simulated $[Ca^{2+}]_{ER}$ curves, it is found that following the initial ER Ca^{2+} release, ER Ca^{2+} release occurs again after $[Ca^{2+}]_{ER}$ reaches a certain level. The $[Ca^{2+}]_{ER}$ value at which the Ca^{2+} release is initiated is denoted by θ_{th}, indicating the $[Ca^{2+}]_{ER}$ threshold at which ER Ca^{2+} release occurs (**Fig. 2**). By comparing $[Ca^{2+}]_{ER}$ curves in **Figure 2A–C**, it can be noticed that θ_{th} is decreased from 85.43 μM to 66.74 μM when caffeine concentration is increased from 3 mM to 10 mM (**Table 1**).

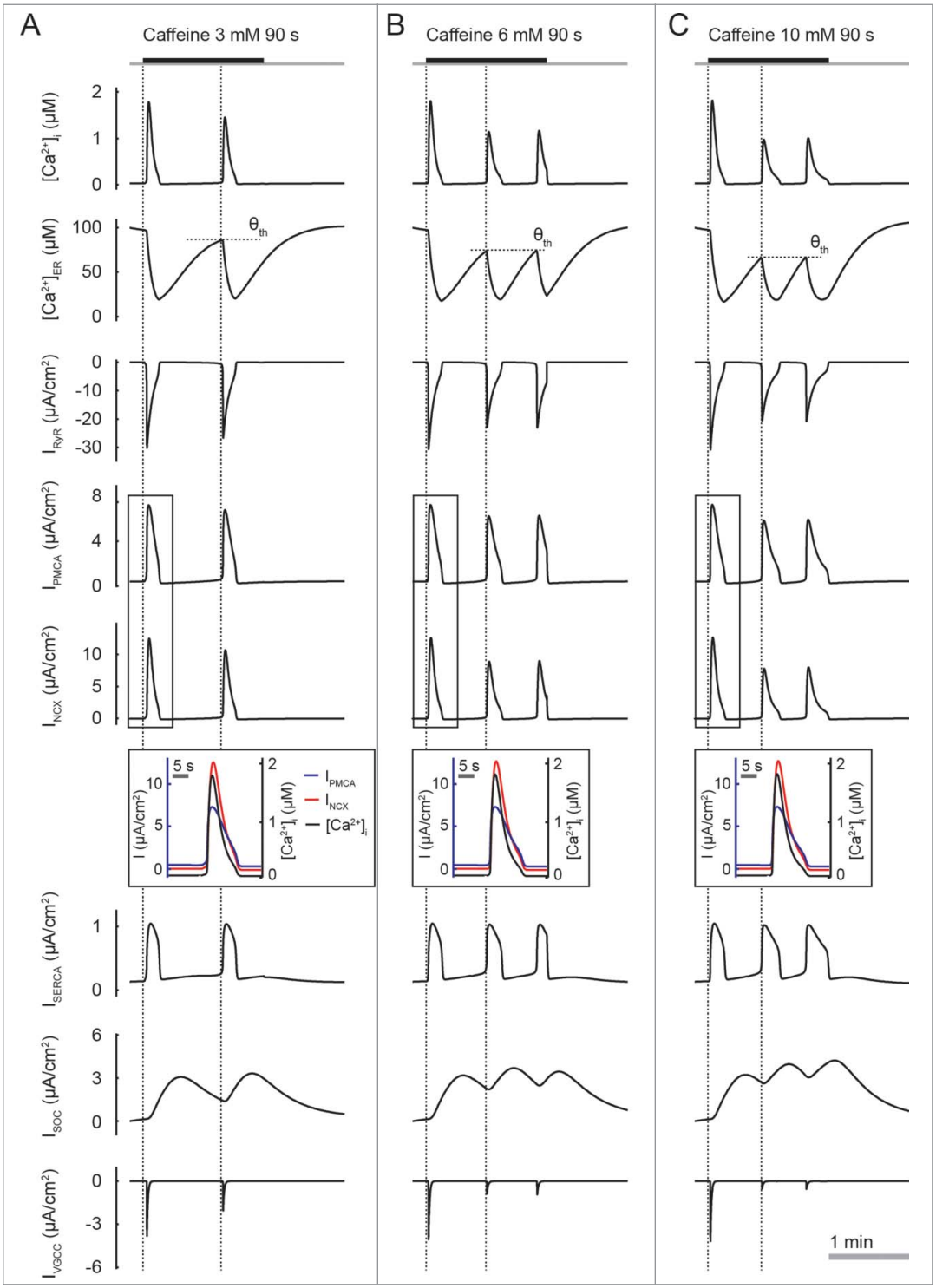

Figure 2. Simulation of caffeine-induced $[Ca^{2+}]_i$ oscillations using the biophysical model of H1 HC. (**A–C**) $[Ca^{2+}]_i$ oscillations induced by 3, 6, 10 mM caffeine (90 s), respectively. Traces shown are the model output of $[Ca^{2+}]_i$, $[Ca^{2+}]_{ER}$ and Ca^{2+} currents mediated by RyR, PMCA, NCX, SERCA, SOC, and L-VGCC, respectively. θ_{th} indicates the $[Ca^{2+}]_{ER}$ threshold at which ER Ca^{2+} release occurs. The insets show dynamic changes of I_{NCX} and I_{PMCA} during the first $[Ca^{2+}]_i$ transient induced by caffeine.

Caffeine effect at different concentrations is represented by using different $K_{d,Ca}$ values, which results in RyR current modulation by influencing P_{RyR} (**Eq. 10**). To further explore the effect of caffeine concentration on caffeine-induced $[Ca^{2+}]_i$ oscillations, dynamic changes of P_{RyR} during caffeine application are plotted together with the corresponding $[Ca^{2+}]_i$ curves (**Fig. 3A–C**). It can be observed that after the first $[Ca^{2+}]_i$ transient, P_{RyR} is decreased to a trough (P_{trough}) when $[Ca^{2+}]_i$

Table 1. The effect of caffeine concentration on caffeine-induced $[Ca^{2+}]_i$ oscillations

	ΔT_{1-2} (s)		A_1 (μM)	A_2 (μM)	A_2/A_1		θ_{th} (μM)
Caffeine (mM)	**E**	**M**	**M**	**M**	**E**	**M**	**M**
3 mM	46.08 ± 3.41	56.72	1.79	1.45	0.82 ± 0.05	0.81	85.43
6 mM	35.40 ± 1.68	43.41	1.81	1.14	0.65 ± 0.04	0.63	73.34
10 mM	28.37 ± 2.30	38.46	1.82	0.98	0.58 ± 0.03	0.54	66.74

E: experimental results, data are presented as mean ± SEM; M: model simulation results.

returns to the basal level, and a high caffeine concentration corresponds to a large P_{trough} value and a quick P_{RyR} increase (**Fig. 3D**). With a large P_{RyR}, the second $[Ca^{2+}]_i$ transient can be induce quickly. Therefore, when the concentration of caffeine is increased, the ΔT_{1-2} interval is decreased (**Table 1**). After the initial release, $[Ca^{2+}]_{ER}$ is increased gradually with time, and a fast second $[Ca^{2+}]_i$ transient is related to a small corresponding θ_{th} value, while a small θ_{th} indicates that only a small amount of ER Ca^{2+} can be released, which results in a small A_2. Hence the value of A_2 is decreased when the caffeine concentration is increased. Simulation results show that A_2 is decreased from 1.45 μM to 0.98 μM as the concentration of caffeine is increased from 3 mM to 10 mM, while the values of A_1 is kept around 1.80 μM. Therefore, the A_2/A_1 ratio is decreased when caffeine concentration is increased (**Table 1**). The above results explain the caffeine concentration dependency of $[Ca^{2+}]_i$ oscillations.

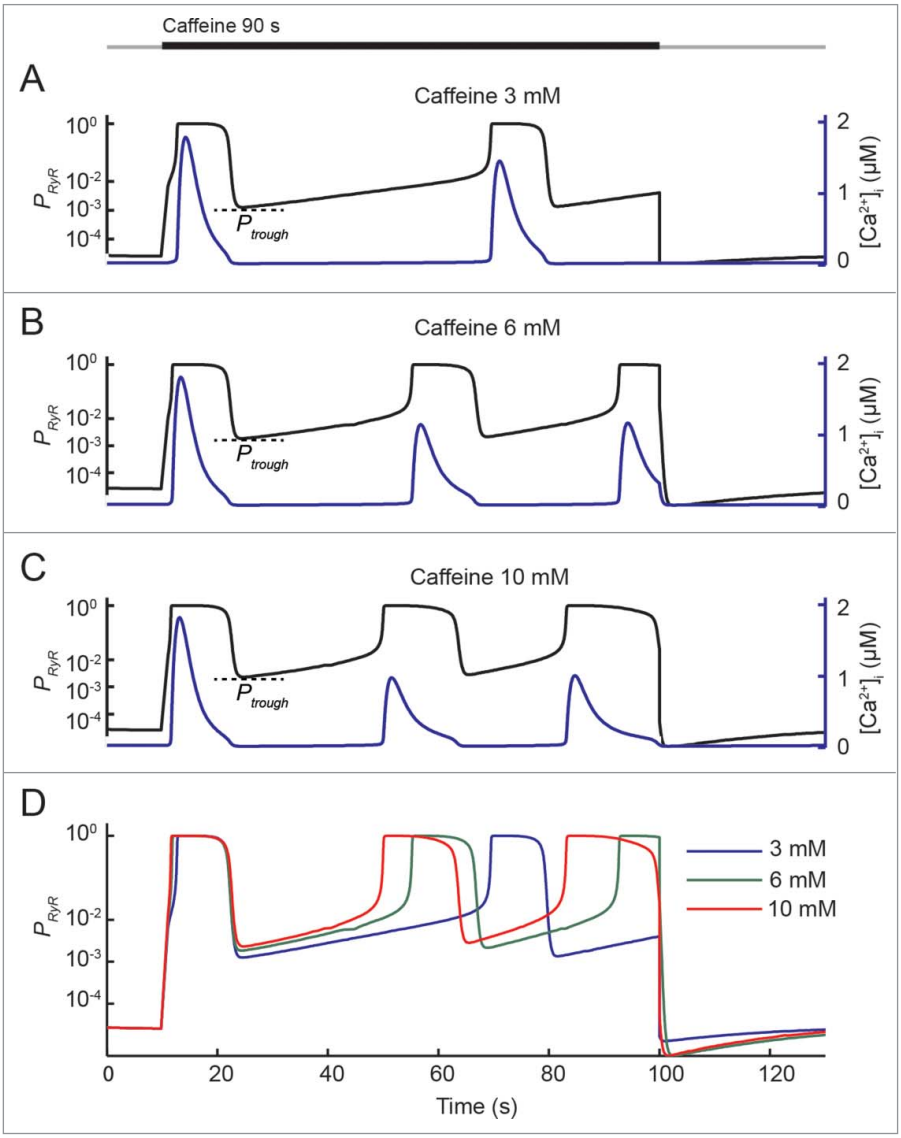

Figure 3. Dynamic changes of RyR open probability (P_{RyR}) during caffeine application. (**A–C**) Simulation output of P_{RyR} (black line, left y-axis) and $[Ca^{2+}]_i$ (blue line, right y-axis) induced by 3, 6, and 10 mM caffeine (90 s), respectively. (**D**) Dynamic changes of P_{RyR} during the application of 3 (blue line), 6 (green line), and 10 mM (red line) caffeine (90 s). P_{RyR} reaches a trough (P_{trough}) after the initial $[Ca^{2+}]_i$ transient. The value of P_{trough} is increased when the concentration of caffeine is increased.

Effect of SOC inhibition on caffeine-induced $[Ca^{2+}]_i$ oscillations

Experimental data from isolated H1 HCs showed that prolonged application of 3 mM caffeine (7 min) induced sustained $[Ca^{2+}]_i$ oscillations in H1 HCs (**Fig. 4A**),[6] and such $[Ca^{2+}]_i$ oscillations were abolished when 2-APB (SOC inhibitor) was co-applied (**Fig. 4B**),[6] suggesting that SOCE is necessary for ER refilling.

Using our model, the above experimental results (**Fig. 4**) are simulated. The effect of 3 mM caffeine is simulated with $K_{d,Ca} = 0.16$ μM, the effect of 2-APB was simulated by setting V_{SOC} (the maximum SOC flux, **Eq. 13**) to 0. As shown in **Figure 5A**, prolonged application of caffeine (3 mM, 7 min) induces sustained $[Ca^{2+}]_i$ oscillations in the model cell, and the oscillation in $[Ca^{2+}]_i$ is concomitant with the periodical release and uptake of ER Ca^{2+}, and SOC current follows the fluctuations of $[Ca^{2+}]_{ER}$. A $[Ca^{2+}]_i$ transient is induced whenever $[Ca^{2+}]_{ER}$ reaches θ_{th}.

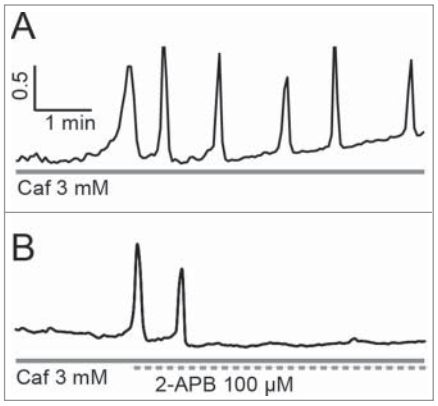

Figure 4. The 2-APB effect on caffeine-induced $[Ca^{2+}]_i$ oscillations. (**A**) $[Ca^{2+}]_i$ oscillations induced by prolonged application of caffeine (3 mM, 7 min). (**B**) After $[Ca^{2+}]_i$ oscillations were induced by caffeine (3 mM), co-application of 2-APB (100 μM) abolished the oscillations immediately.[6]

Although $[Ca^{2+}]_i$ oscillations can be induced by caffeine (3 mM), $[Ca^{2+}]_{ER}$ increase can be immediately stopped when 2-APB is applied. In the presence of 2-APB, SOC is constantly blocked, which abolishes the SOC current (**Fig. 5B**). Without SOCE, $[Ca^{2+}]_{ER}$ is gradually decreased, unable to reach θ_{th}, hence no further Ca^{2+}-induced Ca^{2+} release (CICR) is induced and no $[Ca^{2+}]_i$ transient is generated. This result verifies that SOCE is the main Ca^{2+} source for ER refilling, and the activation of SOC is required for the maintenance of sustained $[Ca^{2+}]_i$ oscillations.

Discussion

In the present study, we constructed a mathematical model to simulate the caffeine-induced $[Ca^{2+}]_i$ oscillations observed in type I horizontal cell of carp retina. Simulated $[Ca^{2+}]_i$ changes closely resemble the experimental observations, the concentration dependence of $\Delta T_{1\text{-}2}$ and A_2/A_1 of the caffeine-induced $[Ca^{2+}]_i$ oscillations can be reproduced. Relevant contributions of RyR, SOC, L-VGCC, NCX, PMCA and SERCA for the caffeine-induced $[Ca^{2+}]_i$ oscillations are suggested. The oscillations in $[Ca^{2+}]_i$ are concomitant with the periodical changes of RyR, PMCA, NCX, SERCA, SOC, and L-VGCC activities.

Simulated $[Ca^{2+}]_{ER}$ curves in **Figures 2 and 5A** show that, continuous application of caffeine leads to repeated release/uptake of ER Ca^{2+}. After each ER Ca^{2+} release, ER is gradually refilled, and subsequent Ca^{2+} release can be induced only when the $[Ca^{2+}]_{ER}$ level is recovered and reaches a certain threshold θ_{th}. When the concentration of caffeine is increased, the value of θ_{th} is decreased (**Fig. 2**, **Table 1**). The concentration-dependent caffeine effect on θ_{th} is consistent with the experimental results reported by Kong et al.[9] In their study, by recording $[Ca^{2+}]_{ER}$ of HEK-293 cells expressing RyR, it was found that the threshold for Ca^{2+} release (θ_{th}) was decreased when the concentration of caffeine was increased.

In carp retinal horizontal cell, Ca^{2+} entering the cytoplasmic is extruded into the extracellular space by both PMCA and NCX.[5] From the simulation output (**Fig. 2**, insets), it can be observed that during caffeine-induced $[Ca^{2+}]_i$ oscillations, Ca^{2+} is extruded mainly by PMCA when $[Ca^{2+}]_i$ is at lower levels; while at higher $[Ca^{2+}]_i$ levels, NCX-mediated Ca^{2+} current is larger than the PMCA Ca^{2+} current. These results confirm the previously reported basic characteristics of PMCA and NCX, i.e., PMCA has higher affinity for Ca^{2+} than NCX, while NCX has higher turnover rate,[10,11] suggesting that PMCA and NCX cooperate to regulate Ca^{2+} signals over a wide $[Ca^{2+}]_i$ range in H1 HC.

In addition to regulating the dynamic changes in $[Ca^{2+}]_i$, PMCA has also been shown to participate in the regulation of resting Ca^{2+} homeostasis. It was reported that in rod-driven bipolar cell of mouse retina, PMCA was involved in the maintenance of the resting $[Ca^{2+}]_i$ levels.[12,13] For our model cell, after

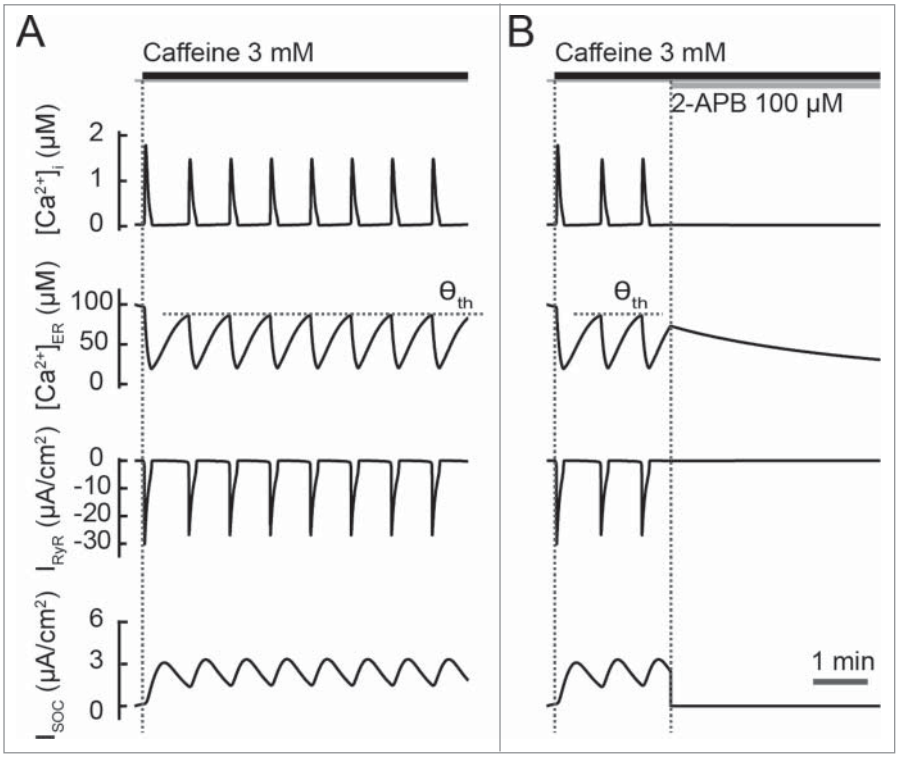

Figure 5. Model output simulating the 2-APB effect on caffeine-induced $[Ca^{2+}]_i$ oscillations. (**A**) Sustained $[Ca^{2+}]_i$ oscillations induced by prolonged caffeine (3 mM, 7 min) application. (**B**) Caffeine (3 mM, 7 min)-induced $[Ca^{2+}]_i$ oscillations are abolished when 2-APB (100 μM) is applied. Traces shown are simulation output of $[Ca^{2+}]_i$, $[Ca^{2+}]_{ER}$ and Ca^{2+} currents mediated by RyR and SOC, respectively. θth indicates the $[Ca^{2+}]_{ER}$ threshold at which ER Ca^{2+} release occurs.

Table 2. Model output in the resting state

Symbol	Value	Unit
I_{NCX}^{REST}	0.0	μA/cm^2
I_{PMCA}^{REST}	0.4	μA/cm^2
I_{SOC}^{REST}	0.4	μA/cm^2
I_{leak}^{REST}	−0.5	μA/cm^2
I_{SERCA}^{REST}	0.1	μA/cm^2
I_{RyR}^{REST}	0.0	μA/cm^2
I_{VGCC}^{REST}	0.0	μA/cm^2
$[Ca^{2+}]_i^{REST}$	28	nM
$[Ca^{2+}]_{ER}^{REST}$	94	μM

the extracellular stimulus is removed, $[Ca^{2+}]_i$ and $[Ca^{2+}]_{ER}$ gradually return to their resting levels, which is independent on the intensity of the previously given stimulation. The levels of $[Ca^{2+}]_i$ and $[Ca^{2+}]_{ER}$, as well as currents carried by different Ca^{2+} components in the resting state are kept within limited ranges (**Table 2**) until a subsequent stimulus is applied. The model output shows that NCX is inactive at rest ($I_{NCX}^{REST} \approx 0.0$ μA/cm^2, **Table 2**) and Ca^{2+} extrusion occurs through PMCA ($I_{PMCA}^{REST} \approx 0.4$ μA/cm^2, **Table 2**). The simulation results suggest that in the resting state, extrusion of cytoplasmic Ca^{2+} depends mainly on PMCA in H1 HC.

It can also be noticed that the SOCE complex is activated at rest ($I_{SOC}^{REST} \approx 0.4$ μA/cm^2, **Table 2**). On the plasma membrane, Ca^{2+} extruded from the cell via PMCA is counterbalanced by Ca^{2+} entering the cell through SOC. On the ER membrane, the passive leakage of Ca^{2+} from the ER ($I_{leak}^{REST} \approx -0.5$ μA/cm^2, **Table 2**) is compensated by SERCA ($I_{SERCA}^{REST} \approx 0.1$ μA/cm^{2}s, **Table 2**) and SOCE complex-mediated Ca^{2+} uptake. Ca^{2+} homeostasis of the model cell is maintained by the activities of PMCA, SOCE complex, ER passive leak, and SERCA, keeping resting $[Ca^{2+}]_i$ and $[Ca^{2+}]_{ER}$ levels at 28 nM and 94 μM, respectively (**Table 2**). The involvement of the SOCE complex in resting Ca^{2+} homeostasis has been reported in cells such as rat primary cortical neurons, mouse mammary epithelial cells, and HEK293 cells.[14-17] In these cells, 2 types of STIM proteins, i.e., STIM1 and STIM2, are expressed on the ER membrane. STIM1 triggers SOCE in response to store-depletion, while STIM2 activates Orai1 upon small fluctuations in $[Ca^{2+}]_{ER}$, keeping resting $[Ca^{2+}]_i$ and $[Ca^{2+}]_{ER}$ stable. Therefore, our simulation results suggest that in addition to ER refilling upon stimuli-induced store depletion (**Fig. 5**), SOC activation in response to minor $[Ca^{2+}]_{ER}$ fluctuation may play a crucial role in maintaining $[Ca^{2+}]_i$ and $[Ca^{2+}]_{ER}$ levels in H1 HC at the resting state.

Experimental results from carp H1 HC show that, L-VGCC was activated during caffeine-induced $[Ca^{2+}]_i$ oscillations.[6] The involvement of L-VGCC suggests that V_m of H1 HC should be depolarized upon caffeine application. Our simulation results show that changes in V_m are concomitant with changes in

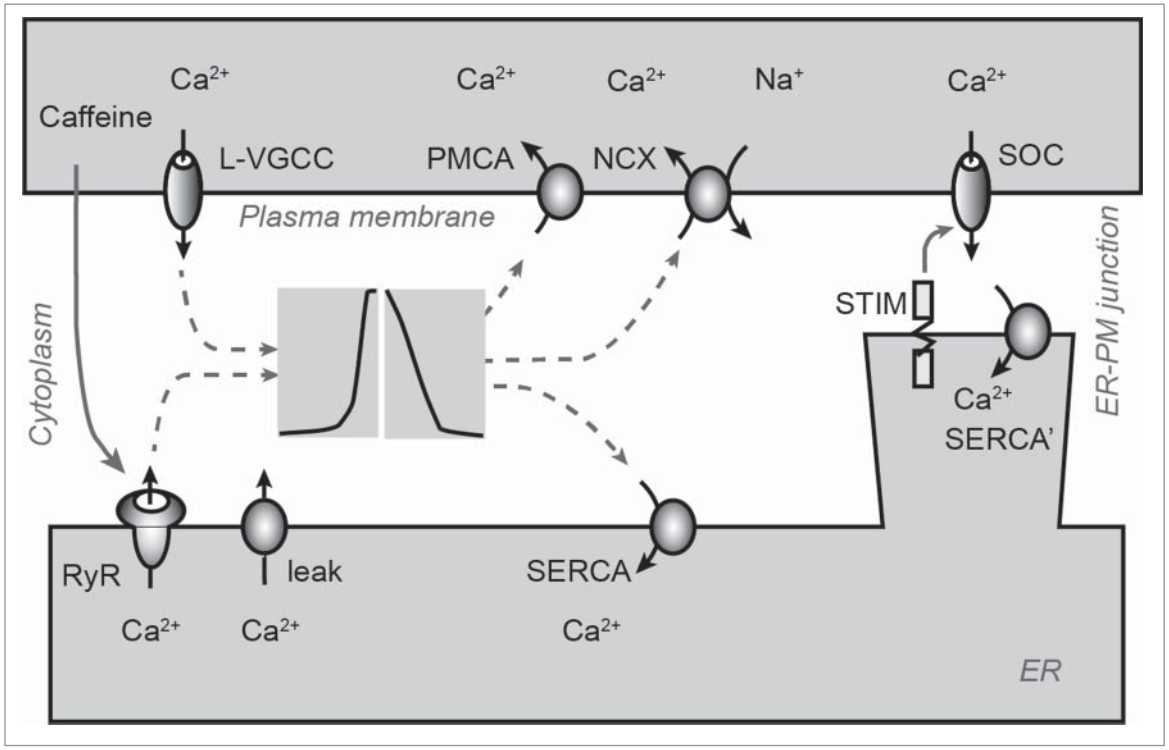

Figure 6. Schematic illustration of Ca^{2+} pathways relevant to caffeine-induced $[Ca^{2+}]_i$ oscillations in carp retinal HC. L-VGCC: L-type voltage-gated Ca^{2+} channel; NCX: Na^+/Ca^{2+} exchanger; PMCA: plasma membrane Ca^{2+}-ATPase; RyR: ryanodine receptor; leak: passive Ca^{2+} leak; SERCA: sarco/endoplasmic reticulum Ca^{2+}-ATPase; ER: endoplasmic reticulum; SOC: store-operated channels; PM: plasma membrane.

$[Ca^{2+}]_i$, and L-VGCC current is activated periodically by membrane depolarization. When the L-VGCC current is blocked by setting $\overline{g}_{Ca}$ to zero, $[Ca^{2+}]_i$ oscillations can still be induced by caffeine (10 mM, 60 s), at the meantime, the A_2/A_1 ratio and $\Delta T_{1\text{-}2}$ interval are slightly increased as compared with control, showing good agreement with experimental data (data not show). Both the simulation and experimental results show that L-VGCC is involved in the caffeine-induced $[Ca^{2+}]_i$ oscillations. However, L-VGCC is not the major source of Ca^{2+} influx during caffeine-induced $[Ca^{2+}]_i$ oscillations, $[Ca^{2+}]_i$ oscillations can be induced when L-VGCC is completely blocked.

Our present study provides fundamental insight into the mechanisms of caffeine-induced $[Ca^{2+}]_i$ oscillations in carp H1 HC, and reveals possible roles of SOC in H1 HC $[Ca^{2+}]_i$ signaling. Further studies are needed to elucidate the molecular identities and functions of SOC in H1 HC physiology.

Methods

Ca^{2+} imaging data

Experimental data were obtained from isolated type I horizontal cell of carp retina using fluo-3-based Ca^{2+} imaging technique. All the materials and methods have been previously reported.[6]

Model description

All simulations were carried out using NEURON software.[18] A cylindrical neuron was constructed, with the $[Ca^{2+}]_i$ dynamics being modeled at the whole-cell level.

The model system is schematically presented in **Figure 6**, which includes Ca^{2+} processes on the plasma membrane (PM), the ER, and the store-operated Ca^{2+} entry (SOCE) complex. Biophysical properties of the neuron membrane are spatially uniform.

The PM processes include the L-VGCC, NCX, and PMCA. L-VGCC mediates Ca^{2+} entry during membrane depolarization, while NCX and PMCA extrude Ca^{2+} from the cytosol into the extracellular space.

The ER processes involve 3 parallel components: Ca^{2+} release from the ER into the cytosol mediated by RyR, passive Ca^{2+} leakage from the ER into the cytosol, and Ca^{2+} uptake from the cytosol into the ER through SERCA.

SOCE is a process in which plasma membrane Ca^{2+} channel (SOC) is activated upon Ca^{2+} store depletion.[19] The SOCE complex is composed of proteins including STIM, SOC, and SERCA. STIM which resides on the ER membrane senses the ER Ca^{2+} content,[20,21] while Orai channels[22-24] and/or TRP channels[25,26] form the SOC on the PM. Upon store depletion, STIM and SOC translocate and cluster at the ER-PM junctions, leading to the formation of the STIM-SOC complexes and SOC activation.[23,27,28] Activated SOC mediates Ca^{2+} influx, and SERCA in the ER-PM junctions uptakes these Ca^{2+} to refill the depleted ER.[29-33]

Besides, voltage-gated K^+ and Na^+ channel conductance also contribute to the regulation of $[Ca^{2+}]_i$ by affecting the neuronal membrane potential, therefore, these processes are also included in our model.

Hence, in our model, Ca^{2+} dynamics can be described as:

$$\begin{aligned}\frac{d[\mathrm{Ca}^{2+}]_\mathrm{i}}{dt} &= f_{cyt}\cdot\left(\frac{I_{\mathrm{Ca}}^{All}}{2\cdot F\cdot vol_{cyt}} + J_{RyR} + J_{leak} - J_{SERCA}\right)\\ \frac{d[\mathrm{Ca}^{2+}]_\mathrm{ER}}{dt} &= f_{ER}\cdot(vol_{cyt}/vol_{ER})\cdot(J_{SOC} + J_{SERCA} - J_{RyR} - J_{leak})\end{aligned} \tag{1}$$

where $[Ca^{2+}]_i$ is the free intracellular Ca^{2+} concentration, $[Ca^{2+}]_{ER}$ is the free Ca^{2+} concentration inside the ER lumen; f_{cyt} and f_{ER} are Ca^{2+} buffering coefficients for cytoplasm and ER, respectively; vol_{cyt} and vol_{ER} are the volumes of the cell (excluding ER) and the ER, respectively; F is the Faraday constant; I_{Ca}^{All} represents the total Ca^{2+} currents across the cell membrane; J_{RyR} represents ER Ca^{2+} release via RyR; J_{leak} represents the passive Ca^{2+} leakage from the ER into the cytosol; J_{SERCA} represents the Ca^{2+} uptake from the cytosol into the ER through SERCA; J_{SOC} represents Ca^{2+} entering the ER through the SOCE complex.

The total Ca^{2+} currents across the plasma membrane are given by:

$$I_{\mathrm{Ca}}^{All} = I_{VGCC} + I_{NCX} + I_{PMCA} \tag{2}$$

where I_{VGCC}, I_{NCX}, and I_{PMCA} denote the Ca^{2+} currents mediated by L-VGCC, NCX, and PMCA respectively.

Ca^{2+} current through L-VGCC (I_{VGCC}) can be described as:[4]

$$\begin{aligned} I_{VGCC} &= \overline{g}_{\mathrm{Ca}}\cdot m_{\mathrm{Ca}}\cdot h_{\mathrm{Ca}}\cdot(V_m - E_{\mathrm{Ca}})\\ \frac{dm_{\mathrm{Ca}}}{dt} &= \alpha_{m_{\mathrm{Ca}}}\cdot(1-m_{\mathrm{Ca}}) - \beta_{m_{\mathrm{Ca}}}\cdot m_{\mathrm{Ca}}\\ \alpha_{m_{\mathrm{Ca}}} &= 33\cdot\frac{92.7 - V_m}{\exp((92.7 - V_m)/9.6) - 1}\\ \beta_{m_{\mathrm{Ca}}} &= 3.3\cdot\exp((-65.2 - V_m)/11.5)\\ h_{\mathrm{Ca}} + \tau_{\mathrm{Ca}}\frac{dh_{\mathrm{Ca}}}{dt} &= K_{\mathrm{Ca}}^n/(K_{\mathrm{Ca}}^n + [\mathrm{Ca}^{2+}]_i^n)\\ E_{\mathrm{Ca}} &= 12.5\cdot\log([\mathrm{Ca}^{2+}]_o/[\mathrm{Ca}^{2+}]_i)\end{aligned} \tag{3}$$

where $\overline{g}_{Ca}$ is the maximum conductance of L-VGCC; m_{Ca} and h_{Ca} are the activation and inactivation variables, respectively; V_m denotes the membrane potential; E_{Ca} stands for the reversal potential of Ca^{2+} current; K_{Ca} is the half-inactivation parameter; n is the Hill coefficient; α and β are forward and backward rate coefficients, respectively; τ_{Ca} represents the inactivation time constant.

Equation 3 shows that the Ca^{2+} dynamics are regulated by V_m, while Ca^{2+} currents together with Na^+ and K^+ currents across the plasma membrane all contribute to the V_m changes. Hence voltage-gated Na^+ conductance and 3 types of K^+ conductance (i.e., delay time rectifying K^+ current, outward rectifying K^+ current, and anomalous rectifying K^+ current), which are expressed in carp retinal HC, are also included in our model.[34]

Current carried by voltage-gated Na^+ channel (I_{Nav}) can be described as:[34]

$$\begin{aligned}
&I_{\mathrm{Na}v} = \overline{g}_{\mathrm{Na}} \cdot m_{\mathrm{Na}}^3 \cdot h_{\mathrm{Na}} \cdot (V_m - E_{\mathrm{Na}}) \\
&\frac{dm_{\mathrm{Na}}}{dt} = \alpha_{m_{\mathrm{Na}}} \cdot (1 - m_{\mathrm{Na}}) - \beta_{m_{\mathrm{Na}}} \cdot m_{\mathrm{Na}} \\
&\alpha_{m_{\mathrm{Na}}} = 40 \cdot \frac{80 - V_m}{\exp((80 - V_m)/15) - 1} \\
&\beta_{m_{\mathrm{Na}}} = 10 \cdot \exp(-V_m/20) \\
&\frac{dh_{\mathrm{Na}}}{dt} = \alpha_{h_{\mathrm{Na}}} \cdot (1 - h_{\mathrm{Na}}) - \beta_{h_{\mathrm{Na}}} \cdot h_{\mathrm{Na}} \\
&\alpha_{h_{\mathrm{Na}}} = 0.01 \cdot \exp(-V_m/30) \\
&\beta_{h_{\mathrm{Na}}} = \frac{2}{\exp((70 - V_m)/10) + 1}
\end{aligned} \tag{4}$$

where $\overline{g}_{\mathrm{Na}}$ is the maximum conductance of the voltage-gated Na^+ channel; m_{Na} and h_{Na} are the activation and inactivation variables, respectively; E_{Na} is the reversal potential of Na^+ current.

Current carried by delay time rectifying K^+ channel (I_{kd}) can be described as:[34]

$$\begin{aligned}
&I_{Kd} = \overline{g}_{Kd} \cdot m_{Kd}^4 \cdot V_K \\
&V_K = V_m - E_K \\
&\frac{dm_{Kd}}{dt} = \alpha_{m_{Kd}} \cdot (1 - m_{Kd}) - \beta_{m_{Kd}} \cdot m_{Kd} \\
&\alpha_{m_{Kd}} = 10 \cdot \frac{120 - V_K}{\exp((120 - V_K)/20) - 1} \\
&\beta_{m_{Kd}} = 5 \cdot \exp(-V_K/20)
\end{aligned} \tag{5}$$

where $\overline{g}_{\mathrm{Kd}}$ is the maximum conductance of the delay time rectifying K^+ channel; m_{Kd} represents the activation variable; E_K is the reversal potential of K^+ current.

Current carried by outward rectifying K^+ channel (I_{Kt}) can be described as:[34]

$$\begin{aligned}
&I_{Kt} = \overline{g}_{Kt} \cdot m_{Kt}^3 \cdot h_{Kt} \cdot V_K \\
&V_K = V_m - E_K \\
&m_{Kt} = \frac{\alpha_{m_{Kt}}}{\alpha_{m_{Kt}} + \beta_{m_{Kt}}} \\
&\alpha_{m_{Kt}} = 40 \cdot \frac{140 - V_K}{\exp((140 - V_K)/15) - 1} \\
&\beta_{m_{Kt}} = 8 \cdot \exp(-V_K/20) \\
&\frac{dh_{Kt}}{dt} = \alpha_{h_{Kt}} \cdot (1 - h_{Kt}) - \beta_{h_{Kt}} \cdot h_{Kt} \\
&\alpha_{h_{Kt}} = 0.01 \cdot \exp(-V_K/20) \\
&\beta_{h_{Kt}} = \frac{2}{\exp((30 - V_K)/10) + 1}
\end{aligned} \tag{6}$$

where $\overline{g}_{\mathrm{Kt}}$ is the maximum conductance of the outward rectifying K^+ channel; m_{Kt} and h_{Kt} are the activation and inactivation variables, respectively.

Current carried by anomalous rectifying K^+ channel (I_{Ka}) can be described as:[34]

$$\begin{aligned}
&I_{\mathrm{K}a} = \overline{g}_{\mathrm{K}a} \cdot m_{\mathrm{K}a}^4 \cdot (V_m - E_K) \\
&m_{\mathrm{K}a} = \frac{1}{1 + \exp\left(\frac{V_m - E_K}{30}\right)}
\end{aligned} \tag{7}$$

where $\overline{g}_{\mathrm{Ka}}$ is the maximum conductance of the anomalous rectifying K^+ channel; m_{Ka} represents the activation variable.

On the plasma membrane, Ca^{2+} extrusion is mediated by NCX and PMCA. Current carried by NCX ($I_{\mathrm{NCX}}^{\mathrm{All}}$) can be described as:[4]

$$\begin{aligned}
I_{\mathrm{NCX}}^{All} = K_{\mathrm{NCX}} \cdot \Bigg\{ &[\mathrm{Na}^+]_i^3 \cdot [\mathrm{Ca}^{2+}]_o \cdot \exp\left(r \cdot V_m \cdot \frac{F}{RT}\right) \\
&- [\mathrm{Na}^+]_o^3 \cdot [\mathrm{Ca}^{2+}]_i \cdot \exp\left[-(1-r) \cdot V_m \cdot \frac{F}{RT}\right] \Bigg\}
\end{aligned} \tag{8}$$

where K_{NCX} is a scaling coefficient; $[Na^+]_i$, $[Na^+]_o$ and $[Ca^{2+}]_o$ are intracellular Na^+ concentration, extracellular Na^+ concentration and extracellular Ca^{2+} concentration, respectively; R and T are the gas constant and the absolute temperature, respectively. The ion exchange ratio is Na^+:Ca^{2+} = 3:1, therefore the currents carried by Na^+ and Ca^{2+} are equal to $3 \times I_{\mathrm{NCX}}^{\mathrm{All}}$ and $-2 \times I_{\mathrm{NCX}}^{\mathrm{All}}$, respectively.

Ca^{2+} extrusion mediated by PMCA can be described as:[4]

$$J_{PMCA} = A_{PMCA} \cdot \frac{[\mathrm{Ca}^{2+}]_i}{K_{PMCA} + [\mathrm{Ca}^{2+}]_i} \tag{9}$$

where J_{PMCA} represents the amount of Ca^{2+} efflux; A_{PMCA} is the maximal pumping rate; K_{PMCA} is the dissociation constant.

RyR, passive ER Ca^{2+} leakage, and SERCA are involved in Ca^{2+} exchange between the cytoplasm and the ER. RyR-mediated Ca^{2+} flux from the ER into the cytosol is described as:[35-37]

$$\begin{aligned}
&J_{RyR} = K_{RyR} \cdot P_{RyR} \cdot ([\mathrm{Ca}^{2+}]_{ER} - [\mathrm{Ca}^{2+}]_i) \\
&P_{RyR} = \frac{[\mathrm{Ca}^{2+}]_i^3}{[\mathrm{Ca}^{2+}]_i^3 + K_{d,\mathrm{Ca}}^3}
\end{aligned} \tag{10}$$

where K_{RyR} is the rate constant; P_{RyR} is the open probability of RyR; $K_{\mathrm{d,Ca}}$ is the activation constant which reflects the $[Ca^{2+}]_i$ sensitivity of CICR.

Passive Ca^{2+} leakage from the ER into the cytosol is described as:[2]

$$J_{leak} = K_{leak} \cdot ([\mathrm{Ca}^{2+}]_{ER} - [\mathrm{Ca}^{2+}]_i) \tag{11}$$

where K_{leak} is the rate constant.

ER Ca^{2+} uptake mediated by SERCA can be described as:[2,37]

$$J_{SERCA} = V_{SERCA} \cdot \frac{[\mathrm{Ca}^{2+}]_i}{[\mathrm{Ca}^{2+}]_i + K_{SERCA1}} \cdot \frac{K_{SERCA2}^6}{[\mathrm{Ca}^{2+}]_{ER}^6 + K_{SERCA2}^6} \tag{12}$$

Table 3. Parameter values used in the model

Component parameter	Symbol	Value	Unit	Reference
L-VGCC				[4]
Half inactivation parameter	K_{Ca}	0.30	μM	
Time constant	τ_{Ca}	2.86	s	
Maximum conductance	$\overline{g}_{Ca}$	120.0	μS/ cm^2	
PMCA				[4]
Maximum pumping rate	A_{PMCA}	0.052	$pM/cm^2/ms$	
Dissociation constant	K_{PMCA}	$7.00e^{-4}$	mM	
Na^+/Ca^{2+} exchanger				[4]
Scaling coefficient	K_{NCX}	0.97	$nA/mmol^4/cm^2$	
	r	0.59		
RyR				[35-37]
Rate constant	K_{RyR}	$3.50e^{-3}$	/ms	
Activation constant	$K_{d,ca}$	1.00	μM	
ER Ca^{2+} leak				[2]
Rate constant	V_{leak}	$5.00e^{-5}$	/ms	
SERCA				[2,37]
Maximum SERCA flux	V_{SERCA}	$1.18e^{-5}$	mM/ms	
Activation constant	K_{SERCA1}	$1.00e^{-4}$	mM	
Inactivation constant	K_{SERCA2}	0.10	mM	
SOC				[38]
Maximum SOCE flux	V_{SOC}	$5.60e^{-5}$	mM/ms	
STIM $[Ca^{2+}]_{ER}$ affinity	K_{SOC}	0.05	mM	
SOCE timescale	τ_{SOC}	20.0	s	
ER Ca^{2+} equation				[39]
ER Ca^{2+} buffering coefficient	f_{ER}	0.01		
ER volume/cell volume (excluding ER)	vol_{ER} / vol_{cyt}	0.15		
$[Ca^{2+}]_i$ equation				[39]
Ca^{2+} buffering coefficient of cytoplasm	f_{cyt}	0.01		
Na^+ and K^+ channels				[39]
	$\overline{g}_{Na}$	120.0	nS	
	$\overline{g}_{Kd}$	0.25	nS	
	$\overline{g}_{Kt}$	2.0	nS	
	$\overline{g}_{Ka}$	50.0	nS	

where V_{SERCA} is the maximum SERCA flux; K_{SERCA1} and K_{SERCA2} are the activation and inactivation constants, respectively.

Table 4. The initial conditions and geometric parameters of the model cell

Component parameter	Symbol	Value	Unit	Reference
Non-zero initial conditions for the model				[39]
	$[Ca^{2+}]_o$	2.0	mM	
	$[Ca^{2+}]_i$ (t = 0)	30.0	nM	
	$[Ca^{2+}]_{ER}$ (t = 0)	100.0	μM	
	V_m (t = 0)	−55.0	mV	
	E_{Na}	70.0	mV	
	$[Na^+]_i$	7.0	mM	
	$[Na^+]_o$	135.0	mM	
	E_K	−55.0	mV	
	$[K^+]_i$	54.4	mM	
	$[K^+]_o$	2.5	mM	
Geometric parameters				[39]
Diameter of the model neuron		20.0	μm	
Length of the model neuron		22.5	μm	

Upon store depletion, SOCE complex can be formed in the ER-PM junctions. Due to the tight coupling between the SOC and SERCA, the majority of Ca^{2+} entering the cytoplasm via SOC is pumped into the ER by SERCA.[29-31] Ca^{2+} entering the ER through the SOCE complex can thus be described as:[38]

$$\begin{aligned} J_{SOC} &= V_{SOC} \cdot P_{SOC} \\ \frac{dP_{SOC}}{dt} &= \frac{P_{SOC}^{\infty} - P_{SOC}}{\tau_{SOC}} \\ P_{SOC}^{\infty} &= \frac{K_{SOC}^4}{K_{SOC}^4 + [Ca^{2+}]_{ER}^4} \end{aligned} \tag{13}$$

where V_{SOC} is the maximum value of the SOC flux, and P_{SOC} represents the fraction of STIM proteins bound to SOC, i.e., the fraction of activated SOC. P_{SOC}^{∞} is the fraction of STIM proteins dissociated from the ER Ca^{2+}. K_{SOC} is the affinity of STIM for $[Ca^{2+}]_{ER}$. τ_{SOC} represents the time constant for the adaptation of STIM to $[Ca^{2+}]_{ER}$ changes.

Parameter values for the above equations used in our model are listed in **Table 3**. The initial conditions (e.g., V_m at $t = 0$) and geometric parameters of the model cell are listed in **Table 4**.

Disclosure of Potential Conflicts of Interest

No potential conflicts of interest were disclosed.

Funding

This work was supported by National Nature Science Foundation of China (grant no. 61375114). The funders had no role in study design, data collection and analysis, decision to publish, or preparation of the manuscript. Funder's website: http://www.nsfc.gov.cn.

References

1. Uhlén P, Fritz N. Biochemistry of calcium oscillations. Biochem Biophys Res Commun 2010; 396:28-32; http://dx.doi.org/10.1016/j.bbrc.2010.02.117
2. Huang SY, Liu Y, Liang PJ. Role of Ca^{2+} store in AMPA-triggered Ca^{2+} dynamics in retinal horizontal cells. Neuroreport 2004; 15:2311-5; PMID:15640746; http://dx.doi.org/10.1097/00001756-200410250-00002
3. Wang XL, Jiang XD, Liang PJ. Intracellular calcium concentration changes initiated by N-methyl-D-aspartic acid receptors in retinal horizontal cells. Neuroreport 2008; 19:675-8; http://dx.doi.org/10.1097/WNR.0b013e3282fb7902
4. Hayashida Y, Yagi T. On the interaction between voltage-gated conductances and Ca^{2+} regulation mechanisms in retinal horizontal cells. J Neurophysiol 2002; 87:172-82; PMID:11784740
5. Hayashida Y, Yagi T, Yasui S. Ca^{2+} regulation by the $Na^{+}Ca^{2+}$ exchanger in retinal horizontal cells depolarized by L-glutamate. Neurosci Res 1998; 31:189-99; PMID:9809664; http://dx.doi.org/10.1016/S0168-0102(98)00037-6
6. Lv T, Gong HQ, Liang PJ. Caffeine-induced Ca^{2+} oscillations in type I horizontal cells of the carp retina and the contribution of the store-operated Ca^{2+} entry pathway. PLoS ONE 2014; 9:e100095; http://dx.doi.org/10.1371/journal.pone.0100095
7. Porta M, Zima AV, Nani A, Diaz-Sylvester PL, Copello JA, Ramos-Franco J, Blatter LA, Fill M. Single ryanodine receptor channel basis of caffeine's action on Ca^{2+} sparks. Biophys J 2011; 100:931-8; PMID:21320437; http://dx.doi.org/10.1016/j.bpj.2011.01.017
8. Sitsapesan R, Williams AJ. Mechanisms of caffeine activation of single calcium-release channels of sheep cardiac sarcoplasmic reticulum. J Physiol 1990; 423:425-39; PMID:2167363
9. Kong H, Jones P, Koop A, Zhang L, Duff H, Chen S. Caffeine induces Ca^{2+} release by reducing the threshold for luminal Ca^{2+} activation of the ryanodine receptor. Biochem J 2008; 414:441-52; PMID:18518861; http://dx.doi.org/10.1042/BJ20080489
10. Brini M, Carafoli E. The plasma membrane Ca^{2+} ATPase and the plasma membrane sodium calcium exchanger cooperate in the regulation of cell calcium. Cold Spring Harb Perspect Biol 2011; 3:a004168; http://dx.doi.org/10.1101/cshperspect.a004168
11. Clapham DE. Calcium signaling. Cell 2007; 131:1047-58; PMID:18083096; http://dx.doi.org/10.1016/j.cell.2007.11.028
12. Wan Q-F, Nixon E, Heidelberger R. Regulation of presynaptic calcium in a mammalian synaptic terminal. J Neurophysiol 2012; 108:3059-67; PMID:22972962; http://dx.doi.org/10.1152/jn.00213.2012
13. Carafoli E. Calcium pump of the plasma membrane. Physiol Rev 1991; 71:129-53; PMID:1986387
14. Brandman O, Liou J, Park WS, Meyer T. STIM2 is a feedback regulator that stabilizes basal cytosolic and endoplasmic reticulum Ca^{2+} levels. Cell 2007; 131:1327-39; PMID:18160041; http://dx.doi.org/10.1016/j.cell.2007.11.039
15. Ross DG, Smart CE, Azimi I, Roberts-Thomson SJ, Monteith GR. Assessment of ORAI1-mediated basal calcium influx in mammary epithelial cells. BMC Cell Biol 2013; 14:57; http://dx.doi.org/10.1186/1471-2121-14-57
16. Gruszczynska-Biegala J, Pomorski P, Wisniewska MB, Kuznicki J. Differential roles for STIM1 and STIM2 in store-operated calcium entry in rat neurons. PLoS One 2011; 6:e19285; http://dx.doi.org/10.1371/journal.pone.0019285
17. Parvez S, Beck A, Peinelt C, Soboloff J, Lis A, Monteilh-Zoller M, Gill DL, Fleig A, Penner R. STIM2 protein mediates distinct store-dependent and store-independent modes of CRAC channel activation. FASEB J 2008; 22:752-61; PMID:17905723; http://dx.doi.org/10.1096/fj.07-9449com
18. Carnevale NT, Hines ML. The NEURON book. Cambridge, UK: Cambridge University Press, 2006.
19. Parekh AB, Putney JW. Store-operated calcium channels. Physiol Rev 2005; 85:757-810; PMID:15788710; http://dx.doi.org/10.1152/physrev.00057.2003
20. Liou J, Kim ML, Do Heo W, Jones JT, Myers JW, Ferrell Jr JE, Meyer T. STIM is a Ca^{2+} sensor essential for Ca^{2+}-store-depletion-triggered Ca^{2+} influx. Curr Biol 2005; 15:1235-41; PMID:16005298; http://dx.doi.org/10.1016/j.cub.2005.05.055
21. Roos J, DiGregorio PJ, Yeromin AV, Ohlsen K, Lioudyno M, Zhang S, Safrina O, Kozak JA, Wagner SL, Cahalan MD. STIM1, an essential and conserved component of store-operated Ca^{2+} channel function. J Cell Biol 2005; 169:435-45; PMID:15866891; http://dx.doi.org/10.1083/jcb.200502019
22. Vig M, Peinelt C, Beck A, Koomoa D, Rabah D, Koblan-Huberson M, Kraft S, Turner H, Fleig A, Penner R. CRACM1 is a plasma membrane protein essential for store-operated Ca^{2+} entry. Science 2006; 312:1220-3; PMID:16645049; http://dx.doi.org/10.1126/science.1127883
23. Zhang SL, Yeromin AV, Zhang XH-F, Yu Y, Safrina O, Penna A, Roos J, Stauderman KA, Cahalan MD. Genome-wide RNAi screen of Ca^{2+} influx identifies genes that regulate Ca^{2+} release-activated Ca^{2+} channel activity. Proc Natl Acad Sci U S A 2006; 103:9357-62; PMID:16751269; http://dx.doi.org/10.1073/pnas.0603161103
24. Yeromin AV, Zhang SL, Jiang W, Yu Y, Safrina O, Cahalan MD. Molecular identification of the CRAC channel by altered ion selectivity in a mutant of Orai. Nature 2006; 443:226-9; PMID:16921385; http://dx.doi.org/10.1038/nature05108
25. Smyth JT, DeHaven WI, Jones BF, Mercer JC, Trebak M, Vazquez G, Putney JW. Emerging perspectives in store-operated Ca^{2+} entry: Roles of Orai, Stim and TRP. Biochim Biophys Acta 2006; 1763:1147-60; PMID:17034882; http://dx.doi.org/10.1016/j.bbamcr.2006.08.050
26. Huang GN, Zeng W, Kim JY, Yuan JP, Han L, Muallem S, Worley PF. STIM1 carboxyl-terminus activates native SOC, I_{crac} and TRPC1 channels. Nat Cell Biol 2006; 8:1003-10; PMID:16906149; http://dx.doi.org/10.1038/ncb1454
27. Peinelt C, Vig M, Koomoa DL, Beck A, Nadler MJ, Koblan-Huberson M, Lis A, Fleig A, Penner R, Kinet J-P. Amplification of CRAC current by STIM1 and CRACM1 (Orai1). Nat Cell Biol 2006; 8:771-3; PMID:16733527; http://dx.doi.org/10.1038/ncb1435
28. Yuan JP, Zeng W, Huang GN, Worley PF, Muallem S. STIM1 heteromultimerizes TRPC channels to determine their function as store-operated channels. Nat Cell Biol 2007; 9:636-45; PMID:17486119; http://dx.doi.org/10.1038/ncb1590
29. Manjarrés IM, Rodríguez-García A, Alonso MT, García-Sancho J. The sarcoendoplasmic reticulum Ca^{2+}-ATPase (SERCA) is the third element in capacitative calcium entry. Cell Calcium 2010; 47:412-8; http://dx.doi.org/10.1016/j.ceca.2010.03.001
30. Manjarrés IM, Alonso MT, García-Sancho J. Calcium entry-calcium refilling (CECR) coupling between store-operated Ca^{2+} entry and sarcoendoplasmic reticulum Ca^{2+}-ATPase. Cell Calcium 2011; 49:153-61; http://dx.doi.org/10.1016/j.ceca.2011.01.007
31. Alonso MT, Manjarrés IM, García-Sancho J. Privileged coupling between Ca^{2+} entry through plasma membrane store-operated Ca^{2+} channels and the endoplasmic reticulum Ca^{2+} pump. Mol Cell Endocrinol 2012; 353:37-44; PMID:21878366; http://dx.doi.org/10.1016/j.mce.2011.08.021
32. Carrasco S, Meyer T. Cracking CRAC. Nat Cell Biol 2010; 12:416-8; http://dx.doi.org/10.1038/ncb0510-416
33. Hong J, Kim M, Lee K, Yuan J, Muallem S. STIM-TRP pathways. In: Groschner K, Graier WF, Romanin C, eds. Store-operated Ca^{2+} entry (SOCE) pathways. Vienna: Springer, 2012:57-72.
34. Wang X-L, Jin X, Liang P-J. Modeling the pre-and post-synaptic components involved in the synaptic modification between cones and horizontal cells in carp retina. Biol Cybern 2007; 96:367-76; PMID:17115217; http://dx.doi.org/10.1007/s00422-006-0123-3
35. Dura M, Zahradník I, Zahradníková A. Kinetics of cardiac RyR channel gating studied at high temporal resolution. Physiol Res 2003; 52:571-8; PMID:14535832
36. Friel D. $[Ca^{2+}]_i$ oscillations in sympathetic neurons: an experimental test of a theoretical model. Biophys J 1995; 68:1752-66; PMID:7612818; http://dx.doi.org/10.1016/S0006-3495(95)80352-8
37. Li Y, Keizer J, Stojilkovic S, Rinzel J. Ca^{2+} excitability of the ER membrane: an explanation for IP_3-induced Ca^{2+} oscillations. Am J Physiol Cell Physiol 1995; 269:C1079-C92; PMID:7491895
38. Croisier H, Tan X, Perez-Zoghbi JF, Sanderson MJ, Sneyd J, Brook BS. Activation of store-operated calcium entry in airway smooth muscle cells: Insight from a mathematical model. PLoS One 2013; 8:e69598; http://dx.doi.org/10.1371/journal.pone.0069598
39. Wang X-L, Jiang X-D, Liang P-J. Intracellular calcium concentration changes initiated by N-methyl-D-aspartic acid receptors in retinal horizontal cells. Neuroreport 2008; 19:675-8; http://dx.doi.org/10.1097/WNR.0b013e3282fb7902